Asad, Bilal; Vaimann, Toomas; Belahcen, Anouar; Kallaste, Ants; Rassõlkin, Anton; Iqbal, Muhammad Naveed

Modified winding function-based model of squirrel cage induction motor for fault diagnostics

Published in:
IET Electric Power Applications

DOI:
10.1049/iet-epa.2019.1002

Published: 01/09/2020

Document Version
Peer-reviewed accepted author manuscript, also known as Final accepted manuscript or Post-print

Please cite the original version:
Asad, B., Vaimann, T., Belahcen, A., Kallaste, A., Rassõlkin, A., & Iqbal, M. N. (2020). Modified winding function-based model of squirrel cage induction motor for fault diagnostics. *IET Electric Power Applications*, *14*(9), 1722-1734. https://doi.org/10.1049/iet-epa.2019.1002

IET Journals
The Institution of Engineering and Technology

Modified Winding Function-based Model of Squirrel Cage Induction Motor for Fault Diagnostics

ISSN 1751-8644
doi: 0000000000
www.ietdl.org

Bilal Asad[1]*, *Toomas Vaimann*[1], *Anouar Belahcen*[2], *Ants Kallaste*[1], *Anton Rassõlkin*[1], *M. Naveed Iqbal*[1]

[1] *Dept. of Electrical Power Engineering and Mechatronics, Tallinn University of Technology, Ehitajate tee 5, Tallinn, Estonia*
[2] *Dept. of Electrical Engineering and Automation, Aalto University, 02150 Espoo, Finland*
* *E-mail: biasad@taltech.ee*

Abstract: This paper presents the modeling and simulation of a squirrel cage induction motor using a modified winding function-based method. The aim of the model is to compute the motor's performance parameters, which are similar to the results obtained using the finite element method (FEM) with a considerably reduced simulation time. This fact can make this model good for iterations based optimization and fault diagnostic algorithms. For this purpose, the actual stator and rotor winding functions and the air gap, with the inclusion of rotor and stator slots, are defined as conditional expressions. The resistances and various inductances are calculated with stepping rotor, saved in lookup tables and are used to calculate speed, torque, and currents of the motor. For the validation of the model, the frequency spectrum of stator current is compared with the one calculated using FEM and measurements taken in the laboratory setup under healthy and broken rotor bar conditions.

1 Introduction

The fault diagnostics of electrical machines at the incipient stage is very important, in order to avoid any catastrophic situation, resulting in complete process failure and huge economic loss. Among various fault diagnostic techniques, such as infrared detection, electromagnetic field inference, acoustics and vibration analysis, motor current signature analysis (MCSA) is very popular because of its simplicity and versatility. It can be used for the estimation of design parameters by considering it in model-dependent techniques such as inverse problem theory. Since electrical machines are complex systems where several parameters are associated with each other, the detection of exact cause of the fault is a challenging task. A lot of work has already been done in the field of fault diagnostics, such as MCSA, which is the most cited in the literature. But due to the inevitable inclusion of complex control algorithms and inverters, these techniques become hazy [1-3] . The conventional techniques become worst when there are multiple faults in the machine. This makes the segregation of faults a challenging task, e.g. the cooling ducts in the rotor can imitate as broken rotor bars [4]. The effective utilization of the model for parameters estimation for control and fault diagnostic can be a promising technique that can avoid the above-mentioned problems. The drawbacks of the model's complexity and required computational power is not a big issue, as the world is moving towards Industry 4.0 and cloud computation, which provides unlimited resources. In the field of inverse problem theory, hardware-in-the-loop or parameters estimation, the motor's global parameters, such as speed, torque, or currents, can be used in an inverse manner to estimate the design parameters, such as inductances and resistances, etc. [5]. The comparison of those estimated parameters with the design parameters can lead to the health estimation of the machine. Hence, the model of the motor should be a good replica of the actual system that is able to simulate various faults in the motor with minimal simulation time. The more accurate the model of the motor is, the better the estimation of the parameters would be. Since most of the faults are degenerative in nature, the model should be fast and sensitive enough to detect the faults at a very early stage. In other words, it should have as few approximations as possible. The motor modeling techniques available in the literature can be divided into two main streams: analytical and numerical. The most common techniques along with their attributes are summarized in Table 1.

The two-axis theory (d-q) based models are very common in literature. The detailed dynamic analysis of wound rotor induction motor under balanced and unbalanced conditions in various reference frames can be found in [6], while a similar kind of analysis without the unbalances is available in [7]. The authors in [8] used the d-q model in conjunction with coupled magnetic circuit theory in order to consider the actual non-sinusoidal distribution of the rotor winding. The d-q modeling-based analysis of broken rotor bars is presented in [9-10] , where the authors transformed the rotor d-q currents into n-loop currents in each iteration.

The authors in [11] used d-q modeling to represent an unbalanced three-phase motor having a stator open circuit, with an equivalent unbalanced two-phase motor to present a new fault-tolerant vector control method. The transient model for the analysis of stator turn faults is presented in [12]. These models are simple to understand, comprehensive, good for dynamic analysis and better for drive systems but they have various simplifications, which make them less attractive in the field of fault diagnostics. These simplifications include the sinusoidal distribution of stator and rotor windings. Although, they can be converted to the actual windings but at the cost of increased complexity. The constant air gap by referring stator and rotor parameters on either side eliminates spatial harmonics, which are very important for fault diagnostics. This leads to constant inductances, eliminating their dependency on the rotor position and the non-linear nature of magnetic material. Most of the above-mentioned problems can be resolved by considering the multiple coupled circuit (MCC) theory, which allows the modeling of the unbalanced machine. The authors of [15] used winding function analysis (WFA) for modeling a three-phase squirrel cage induction motor (SQIM) with stator inter-turn short circuit fault. In [13], the authors used it to simulate SQIM with broken rotor bars. The analysis of various faults, such as stator phase disconnection, broken bars, and broken end rings, is presented in [14], while the approach was used for the analysis of adjustable speed drive applications in [33]-[34]. The authors of [35] used this technique to model a permanent magnet machine with a fractional slot concentrated winding. The air gap is considered as constant in the majority of WFA based papers, which do not allow to simulate eccentricity faults and the rotor slot harmonics are potentially ignored. Moreover, the uniform air gap makes it difficult

to deal with material nonlinearities. These problems can be solved by using the modified winding function analysis (MWFA) method, where the slot openings of the stator and rotor can be considered by making the air gap as a function of the stator and rotor position. The authors in [36] extended the WFA based method to simulate electrical machines with a non-uniform air gap. The use of the MWFA

Table 1 The common modeling techniques with corresponding attributes

Technique	Variants	Faults and applications	Attributes
D-Q Modeling	• d-q • Modified d-q	• Drives • Dynamic analysis [6]-[8] • Broken rotor bars [9], [10] • Broken end rings [9], [10] • Stator open circuit [11] • Stator short circuit [12]	**Pros:** • Simple • Comprehensive • Provides good equations for parameters estimation • Good for control and drives **Cons:** • Negligible saturation • Uniform air gap • Sinusoidal stator winding • No inter-bar currents • No spatial harmonics • No eccentricity faults • No skin effects • Difficult to deal with asymmetries, which are inevitable with the fault
Multiple coupled circuits (MCC)	• Winding function analysis (WFA) • Modified winding function analysis (MWFA) • Extended Modified winding function analysis (MWFA)	• Broken rotor bars [13] • Broken end rings • Stator open circuit [14] • Stator short circuit [15] • Dynamic eccentricity [16] • Static eccentricity [17] • Corroded rotor bars • Bearing faults	**Pros:** • Non-uniform air gap • Practical winding functions • Saturation can be defined analytically • Various kind of faults can be simulated • Low computation time as compared to FEM • A very good tradeoff between complexity and accuracy **Cons:** • Some geometrical constraints are difficult to handle, such as cooling ducts in stator or rotor
Magnetic coupling	• Magnetic reluctance method	• Broken rotor bars [18] • Broken end rings [19] • Stator open circuit • Stator short circuit [18] • Dynamic eccentricity [20] • Static eccentricity [20]	**Pros:** • Can include spatial dependencies • Computationally less intense than FEM but more than MCC • It can include geometry, material parameters, and winding distribution **Cons:** • Since all slots need to be modeled and the faulty machine is no longer symmetrical, the model becomes very complex
Others analytical	• Generalized harmonic analysis [21]-[23] • Concordia transformation [24] • Voltage behind reactance [25] • Convolution based [26]	• Winding faults [16], [17] • Losses and torque pulsation [23] • Stator short circuit and broken rotor bars [24][25] • Broken rotor bars [26]	**Pros:** • Concordia transformation reduces the number of state variables. • The convolution-based method is fast and allows to handle various non-ideal parameters **Cons:** • The generalized harmonic analysis limits the number of harmonics taken into consideration • Inclusion of non-uniform air gap is not straightforward in two-axis theory-based models • Nonlinearities will increase the complexity of analytical equations in two-axis theory-based models • Concordia transform inherits the problems of d-q modeling • Convolution theorem inherits the drawbacks of FFT whilet the air gap is taken as constant
Finite element analysis	• Static • Time-stepping • Quasi-static • 2D • 3D	• Broken rotor bars [27], [28] • Broken end rings [28] • Stator open circuit [29] • Stator short circuit [30] • Dynamic eccentricity [31] • Static eccentricity [32]	**Pros:** • Complex geometries can be considered • Non-linearities, such as saturation, skinning effect, and non-idealities can be considered • All kind of faults can be simulated The combination of FEM and analytical modeling can be a good choice **Cons:** • The computational complexity is the biggest problem and becomes worst in case fault diagnostics where symmetry is no longer present. The problem becomes worst for 3D analysis. Unsuitable for hardware-in-the-loop environment and inverse problem theory

to model the stator and rotor slot effects for speed sensor-less drive systems is presented in [37]. The static and dynamic eccentricities are presented in [17] and [16] respectively. Unlike [37], where the air gap permeance is approximated by cosine series functions, [38] used the actual stator and rotor slot opening functions and a medium magnetic equipotential surface to simulate the machine. By doing so, the authors obtained results very close to the ones obtained from FEM. The simulation time was further reduced by exploiting the symmetry of the rotor cage, which is not true in case of faulty machines. The analytical models show their limitations, while dealing with complex geometries, material properties, and non-linearities, etc. These problems can leave them unsuitable for fault diagnostics, making some advanced techniques inevitable. The FEM has been extensively used in literature to tackle the mentioned problems. The authors in [39] used FEM to model an induction machine with the inclusion of eddy current and hysteresis in steel laminations. The magnetic field analysis of induction motors with cooling ducts is presented in [40]. The authors of [41] used this technique to study the vibrations in an induction motor with a 2D magnetic solution and coupled with a 3D mechanical model of the stator, to reduce the complexity. For the same purpose, the authors of [42] used a quasi 3D FEM to compute the magnetic forces on stator end windings of an induction machine. Although the FEM based models are very close approximations of the actual systems they present a high level of complexity and thus unaffordable computation time, especially in real-time applications. Since under faulty condition the motor becomes unsymmetrical, the solution of the complete geometry is necessary, causing an extensive increase in the number of mesh elements. Although modern-day computers are powerful, still the FEM based models require considerable time for simulation, which makes them unsuitable for the use in model dependent diagnostic algorithms.

In this paper, a detailed analytical model of a squirrel cage induction motor using MWFA is presented with the following attractive features:

- Unlike most of the authors who have defined first strong harmonics in the form of Fourier sum, which makes the spectrum bandwidth limited. In the proposed model, all winding and air gap functions are defined as notational or conditional expressions. This approach makes the model independent of the selective number of frequency components in the flux density and ensures the contribution of complete spectrum.
- The air gap is made as a function of rotor and stator slot openings, which includes the spatial harmonics.
- The inclusion of rotor slot harmonics makes the model suitable for sensor-less speed drive systems.
- The model is so generic that almost all kinds of faults such as broken rotor bars, static and dynamic eccentricity and stator short circuits can be simulated. However, in this paper, the broken bars are discussed.
- The very short simulation time as compared to that taken by FEM makes the model suitable for advanced model dependent diagnostic algorithms.
- The achieved results are compared with the ones from the FEM model and measurements taken from the practical setup.
- The model allows to include magnetic saturation effects, which can be considered as a potential improvement.
- The division of the model into offline and online parts can further reduce the complexity by avoiding the unnecessary computations for various fault simulations.

This paper is organized in the way that section 2 presents the generalized mathematical model of the machine. The block diagram showing the implementation strategy is presented in section 3. The impact of stator and rotor slots on the air gap permeance function is presented in section 4, while the winding functions and calculation of various inductances are discussed in section 5. Section 6 presents the simulation results, while the practical measurement setup and the validation of the results are presented in sections 7 and 8 respectively. The conclusions are discussed in section 9.

2 Mathematical Model

According to magnetically coupled circuit model, the voltage equations of the stationary three-phase stator and rotating n-phase rotor can be described as:

$$\boldsymbol{V}_s = \boldsymbol{I}_s \boldsymbol{R}_s + \frac{d}{dt}\boldsymbol{\phi}_s \tag{1}$$

$$\boldsymbol{0} = \boldsymbol{I}_r \boldsymbol{R}_r + \frac{d}{dt}\boldsymbol{\phi}_r \tag{2}$$

where $\boldsymbol{V}_s$, $\boldsymbol{I}_s$, $\boldsymbol{I}_r$, $\boldsymbol{R}_s$, $\boldsymbol{R}_r$, $\boldsymbol{\phi}_s$ and $\boldsymbol{\phi}_r$ are vectors expressing voltage, current, resistance, and fluxe of each stator phase and rotor bar. The stator and rotor fluxes can be represented as:

$$\boldsymbol{\phi}_s = \boldsymbol{L}_{ss}\boldsymbol{I}_s + \boldsymbol{L}_{sr}\boldsymbol{I}_r \tag{3}$$

$$\boldsymbol{\phi}_r = \boldsymbol{L}_{rs}\boldsymbol{I}_s + \boldsymbol{L}_{rr}\boldsymbol{I}_r = \boldsymbol{L}_{sr}^T\boldsymbol{I}_s + \boldsymbol{L}_{rr}\boldsymbol{I}_r \tag{4}$$

where $\boldsymbol{L}_{ss}$, $\boldsymbol{L}_{sr}$, $\boldsymbol{L}_{rs}$, and $\boldsymbol{L}_{rr}$ are the stator-stator, stator-rotor, rotor-stator, and rotor-rotor self and mutual inductance matrices described as follows:

$$\boldsymbol{L}_{ss} = \begin{bmatrix} L_{aas} & L_{abs} & L_{acs} \\ L_{bas} & L_{bbs} & L_{bcs} \\ L_{cas} & L_{cbs} & L_{ccs} \end{bmatrix} \tag{5}$$

$$\boldsymbol{L}_{sr} = \begin{bmatrix} L_{ar_1} & L_{ar_2} & \cdots & L_{ar_i} & \cdots & L_{ar_n} & L_{ar_e} \\ L_{br_1} & L_{br_2} & \cdots & L_{br_i} & \cdots & L_{ar_n} & L_{ar_e} \\ L_{cr_1} & L_{cr_2} & \cdots & L_{cr_i} & \cdots & L_{ar_n} & L_{ar_e} \end{bmatrix} \tag{6}$$

$$\boldsymbol{L}_{rr} = \begin{bmatrix} L_{r_1r_1} & L_{r_1r_2} & \cdots & L_{r_1r_i} & \cdots & L_{r_1r_n} & L_{r_1r_e} \\ L_{r_2r_1} & L_{r_2r_2} & \cdots & L_{r_2r_i} & \cdots & L_{r_2r_n} & L_{r_2r_e} \\ \vdots & \vdots & \vdots & \vdots & \vdots & \vdots & \vdots \\ L_{r_ir_1} & L_{r_ir_2} & \cdots & L_{r_ir_i} & \cdots & L_{r_ir_n} & L_{r_ir_e} \\ \vdots & \vdots & \vdots & \vdots & \vdots & \vdots & \vdots \\ L_{r_nr_1} & L_{r_nr_2} & \cdots & L_{r_nr_i} & \cdots & L_{r_nr_n} & L_{r_nr_e} \\ L_{r_er_1} & L_{r_er_2} & \cdots & L_{r_er_i} & \cdots & L_{r_er_n} & L_{r_er_e} \end{bmatrix} \tag{7}$$

In the matrices, the elements with subscripts a, b, c , r and r_e represent stator's three phases, rotor bars and rotor end ring related entries respectively.

Under the symmetrical condition, the last rows and columns containing only end ring resistance and mutual inductances can be neglected, because the net current in the end ring is zero, but it can lead to a problem of singularities in the simulation, while taking the

$$R_{rr} = \begin{bmatrix} 2(R_b+r_e) & -R_b & 0 & 0 & \cdots & 0 & \cdots & 0 & -R_b & -r_e \\ -R_b & 2(R_b+r_e) & -R_b & 0 & \cdots & 0 & \cdots & 0 & 0 & -r_e \\ 0 & -R_b & 2(R_b+r_e) & -R_b & \cdots & 0 & \cdots & 0 & 0 & -r_e \\ \vdots & \vdots & \vdots & \vdots & \vdots & \vdots & \vdots & \vdots & \vdots & \vdots \\ 0 & 0 & 0 & 0 & \cdots & 0 & \cdots & 2(R_b+r_e) & -R_b & -r_e \\ -R_b & 0 & 0 & 0 & \cdots & 0 & \cdots & -R_b & 2(R_b+r_e) & -r_e \\ -r_e & -r_e & -r_e & -r_e & \cdots & -r_e & \cdots & -r_e & -r_e & n_br_e \end{bmatrix} \tag{8}$$

inverse of the matrices. Moreover, they can be used to simulate end ring related asymmetries and faults.

For the ease of implementation, all these matrices can be grouped together.

$$\boldsymbol{V}_s = \begin{bmatrix} v_{as} & v_{bs} & v_{cs} \end{bmatrix}^T \tag{9}$$

$$\boldsymbol{I}_s = \begin{bmatrix} i_{as} & i_{bs} & i_{cs} \end{bmatrix}^T \tag{10}$$

$$\boldsymbol{I}_r = \begin{bmatrix} i_{r1} & i_{r2} & \cdots & i_{rn} & i_{re} \end{bmatrix}^T \tag{11}$$

$$\boldsymbol{L} = \begin{bmatrix} \boldsymbol{L}_{ss} & \boldsymbol{L}_{sr} \\ \boldsymbol{L}_{rs} & \boldsymbol{L}_{rr} \end{bmatrix} \tag{12}$$

Leading to the matrix equation:

$$\begin{bmatrix} \boldsymbol{V}_s \\ \boldsymbol{0} \end{bmatrix} = \begin{bmatrix} \boldsymbol{R}_s & \boldsymbol{0} \\ \boldsymbol{0} & \boldsymbol{R}_r \end{bmatrix} \begin{bmatrix} \boldsymbol{I}_s \\ \boldsymbol{I}_r \end{bmatrix} + \frac{d}{dt} \begin{bmatrix} \boldsymbol{L}_{ss} & \boldsymbol{L}_{sr} \\ \boldsymbol{L}_{rs} & \boldsymbol{L}_{rr} \end{bmatrix} \tag{13}$$

From where currents and torque are calculated as:

$$\begin{bmatrix} \boldsymbol{I}_s \\ \boldsymbol{I}_r \end{bmatrix} = \begin{bmatrix} \boldsymbol{L}_{ss} & \boldsymbol{L}_{sr} \\ \boldsymbol{L}_{rs} & \boldsymbol{L}_{rr} \end{bmatrix}^{-1} \int \left[\begin{bmatrix} \boldsymbol{V}_s \\ \boldsymbol{0} \end{bmatrix} - \begin{bmatrix} \boldsymbol{R}_s & \boldsymbol{0} \\ \boldsymbol{0} & \boldsymbol{R}_s \end{bmatrix} \begin{bmatrix} \boldsymbol{I}_s \\ \boldsymbol{I}_r \end{bmatrix} \right] dt \tag{14}$$

$$T_e = I_s^T \left(\frac{d}{d\theta} L_{sr} \right) I_r \tag{15}$$

In the matrices form:

$$T_e = \frac{1}{2} \left(\frac{p}{2} \right) \begin{bmatrix} \boldsymbol{I}_s \\ \boldsymbol{I}_r \end{bmatrix}^T \frac{d}{d\theta} \begin{bmatrix} \boldsymbol{L}_{ss} & \boldsymbol{L}_{sr} \\ \boldsymbol{L}_{rs} & \boldsymbol{L}_{rr} \end{bmatrix} \begin{bmatrix} \boldsymbol{I}_s \\ \boldsymbol{I}_r \end{bmatrix} \tag{16}$$

It is worth mentioning here that the derivatives of L_{ss} and L_{rr} are no longer zero as they are the functions of air gap which is changing with rotor position.

The rotor bar and stator phase resistances are calculated by using the formula:

$$R = \left(\frac{\rho l}{A} \right) \tag{17}$$

where ρ is the resistivity, A is the effective slot area and l is the slot length.

The per turn length (l_{pt}) of stator coil is calculated by adding the length of the end winding (l_{ew}) with the effective length (l) of the machine.

$$l_{pt} = l + l_{ew} \tag{18}$$

The dynamic equation of the rotor is given by:

$$J \frac{d}{d\theta} \omega_m = T_e - T_L - B\omega_m \tag{19}$$

where B is the friction coefficient, ω_m is the rotor angular speed, J is the rotor's moment of inertia, T_e and T_L are the generated and load torques respectively.

3 Block Diagram and Description

The implementation strategy can be divided into two steps: offline calculations(Matlab script) saved as 3D lookup tables and online calculations (Simulink), as presented in the block diagram shown in Fig. 1. In the offline calculations, the geometry and corresponding stator and rotor winding functions are considered as input parameters. The slots geometry is used to calculate the resistances matrices by considering the number of conductors, area of slot and filling factor, which is 0.60 in this case. The rotor and stator leakage inductances are calculated using analytical equations discussed in [43]. The stator end windings are compensated by increasing the per turn length as given in (18) and by including the end winding leakage inductance L_{ew} (0.34 mH) which is calculated using (VII) in appendix.

Since the inductances are the function of the air gap, which changes with the change in the rotor position, the rotor's mechanical angle (2π) is divided into ($n \times Q_s \times n_b$) steps, where n is an integer while Q_s and n_b are the number of stator and rotor slots respectively. All the parameters are calculated at each position of stepping rotor.

The calculated data at each rotor position corresponds to a 2D matrix as shown by (5)-(8). All those 2D matrices are stacked in a 3D lookup table, which are called as a function of rotor position and performance parameters, such as currents, fluxes, torque, and speed, are calculated. The integration of the rotor speed gives the new rotor position, which is used to change the index of the lookup table to for the corresponding 2D matrix.

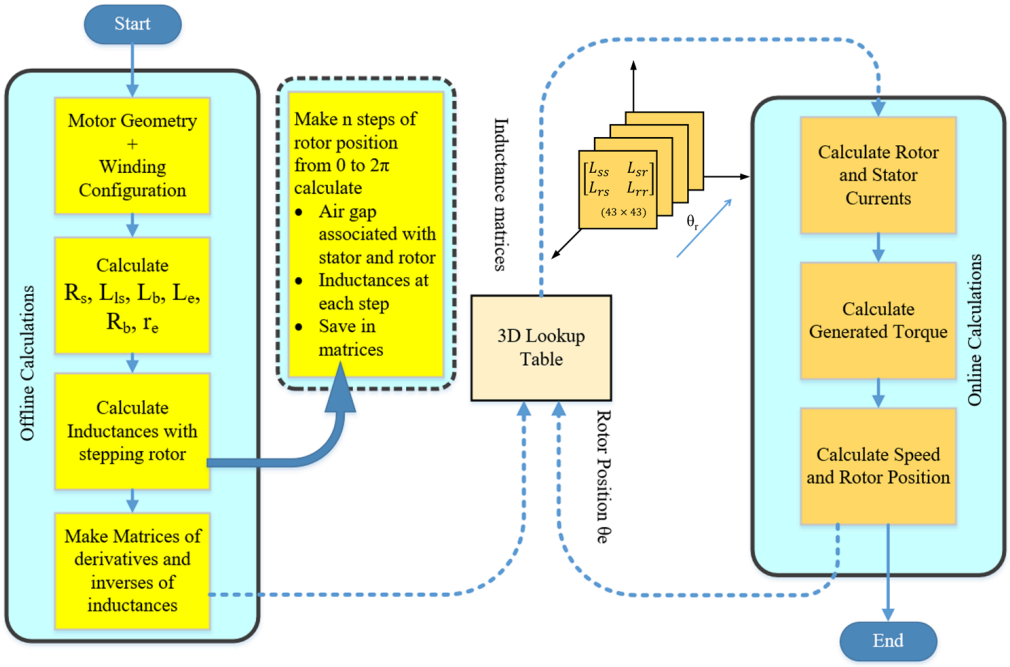

Fig. 1: The flowchart diagram of modeling and simulation

4 Air Gap Permenace Function

The air gap permeance function $P(\theta, \alpha)$ can be defined as:

$$P(\theta, \alpha) = \frac{1}{g_s(\theta) + g_r(\theta, \alpha)} \tag{20}$$

where $g_s(\theta)$, $g_r(\theta, \alpha)$, $g_s(\theta) + g_r(\theta, \alpha)$, and $P(\theta, \alpha)$ are air gaps associated with the stator, rotor, equivalent and the inverse air gap function in stator frame of reference respectively. Moreover, θ is the angle of stator from any fixed reference point and α is the rotor angle in stator reference frame.

The stator and rotor linked air gaps are calculated in the way that the center of the machine's air gap is taken as a reference line. In this way, the total air gap can be divided into stator and rotor associated air gaps. The slot opening without any conductor of winding on the stator side is used to change the air gap as a function of the stator's mechanical angle. This change is in the form of increase in the air gap, equivalent to the height of the slot opening without winding. Similarly, rotor bar depth is used to change the rotor's associated air gap. Both air gaps are added together to get the equivalent air gap at each rotor position. These air gap functions for one stator and rotor slot can be defined as follows:

$$g_s(\theta) = \begin{cases} r_g + h_{11} & 0 \leq \theta \leq B_{11} \\ r_g & B_{11} < \theta \leq (B_{11} + B_{tt}) \end{cases} \tag{21}$$

$$g_r(\theta, \alpha) = \begin{cases} r_g + h_{21} & 0 \leq \theta \leq B_{21} \\ r_g & B_{21} < \theta \leq (B_{11} + B_{rt}) \end{cases} \tag{22}$$

where B_{11}, B_{tt}, B_{21}, B_{rt}, h_{11}, and h_{21} are the width of the stator slot opening, stator tooth tip, rotor slot opening, rotor tooth tip, stator slot depth without winding, and the rotor bar depth respectively as given in Table 2. Fig. 2 shows the stator and rotor associated air gaps until (2π) electrical angle, which is equivalent to half of the mechanical geometry, since the machine is four-pole. The net air gap with its inverse function at a particular position is also shown in the figure, where the distinguished (extended) lines are representing the points where rotor and stator slots overlap with each other. r_g is the average air gap radius and can be calculated as:

$$r = \frac{(D_s - D_r)}{2} \tag{23}$$

For a more accurate representation of radius, (23) can be modified as follows:

$$r_g(\theta, \alpha) = r + \frac{g_s(\theta) + g_r(\theta, \alpha)}{2} \tag{24}$$

5 Winding Function and Inductances Calculation

The inductances are dependent on the air gap permeance $P(\theta, \alpha)$, which is not a constant but a function of stator and rotor slot openings as described in (20)-(22). The winding function can be described as [37]:

$$N_i(\theta) = \left(n_i(\theta) - \frac{< P n_i >}{< P >} \right) \tag{25}$$

where n_i, N_i and P are the turn function, winding function and the air gap permeance function respectively. For a p pole machine, the average or mean value of any function $f(\theta_e)$ can be calculated as shown below;

$$< f >= \frac{1}{p\pi} \int_0^{p\pi} f(\theta_e) d\theta_e \tag{26}$$

The stator and rotor winding functions are shown in Fig. 3, which are calculated using conditional analytic expressions (appendix VIII). Each stator slot contains 17 conductors with a coil pitch equivalent to 12 slots. The rotor winding function is calculated by considering one conductor per slot. The winding function based inductances, while considering constant radius, can be calculated using the following equation.

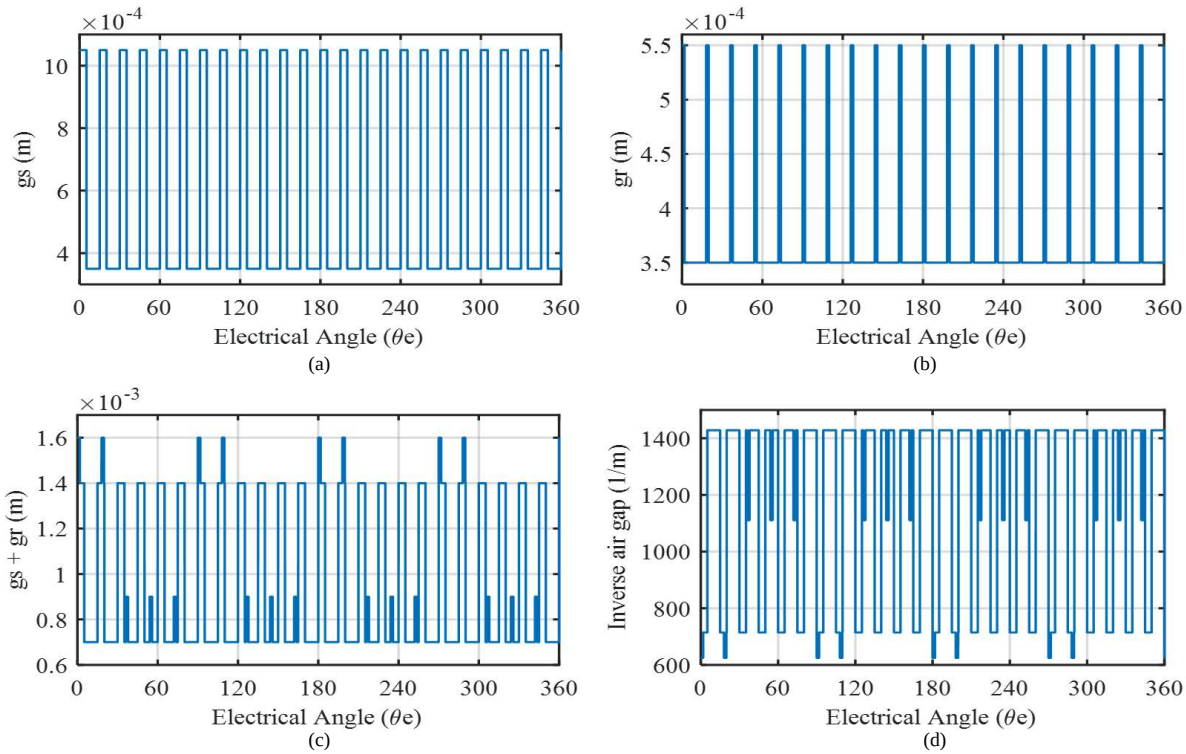

Fig. 2: The air gap function of (a) the stator (g_s), (b) the rotor (g_r), (c) the net equivalent $(g_s + g_r)$ and (d) the inverse air gap function at some specific rotor position.

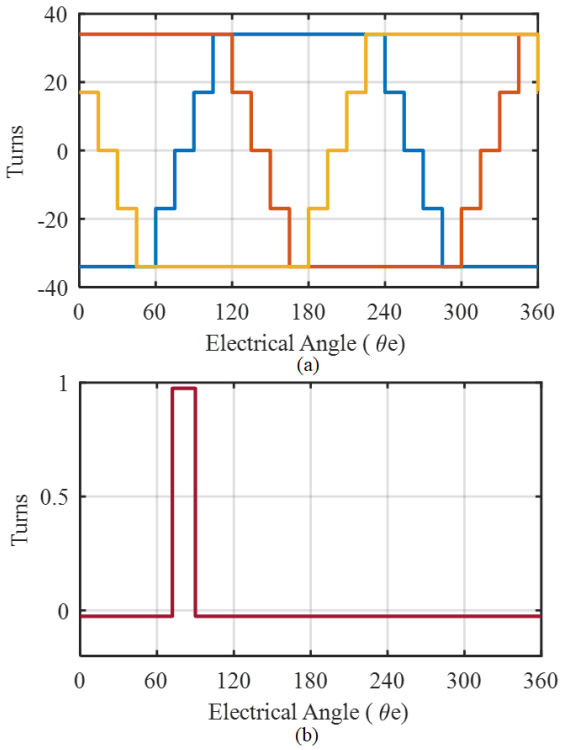

Fig. 3: The winding functions (a) three phase stator, (b) one loop of rotor.

$$L_{ij}(\theta) = \mu_o rl \int_0^{2\pi} P(\theta,\alpha) N_i(\theta,\alpha) n_j(\theta,\alpha) d\theta \qquad (27)$$

This equation can be written as a mean value function as in (26).

$$L_{ij}(\theta) = 2\pi\mu_o rl < P(\theta,\alpha) N_i(\theta,\alpha) n_j(\theta,\alpha) > \qquad (28)$$

Or in the form of turn functions:

$$L_{ij}(\theta) = 2\pi\mu_o rl[< P(\theta,\alpha) n_i(\theta,\alpha) n_j(\theta,\alpha) > - \frac{< P(\theta,\alpha) n_i(\theta,\alpha) >< P(\theta,\alpha) n_j(\theta,\alpha) >}{< P(\theta,\alpha) >}] \qquad (29)$$

If the average radius of air gap is considered as (24) then:

$$L_{ij}(\theta) = 2\pi\mu_o l < r_g(\theta,\alpha) P(\theta,\alpha) N_i(\theta,\alpha) n_j(\theta,\alpha) > \qquad (30)$$

The equation (30) describes that the inductances are the function of average air gap radius, air gap permeance function and winding functions and all of them depend upon the relative position of stator and rotor. Unlike most of the inductance equations in literature, the elimination of integrators with mean value function as in (30) (appendix II-V) further reduces the complexity and increases the ease of its implementation. Various inductances, such as stator-stator self, stator-stator mutual, stator-rotor mutual, and rotor-rotor self, are shown in Fig. 4.

All these inductances are calculated with a considerable number of rotor steps $(10\times n_b \times Q_s)$ to improve the resolution, where nb and Qs are 40 and 48 respectively, taken from machine under investigation. The corresponding derivatives of the inductances shown in Fig. 4 are presented in Fig. 5. The rate of change of inductances with respect to rotor position (derivative) is no longer zero. It oscillates across the zero lines and increases with the increase in the air gap variations. The calculated results for inductances, their derivatives, and inverses are saved in matrices generating three 3D lookup tables each having a dimension of $(44\times44\times19200)$. The resistances and leakage inductances are calculated based on geometry and number of turns on stator and rotor side as given in Table 2.

Table 2 Slots dimensions of the machine under investigation

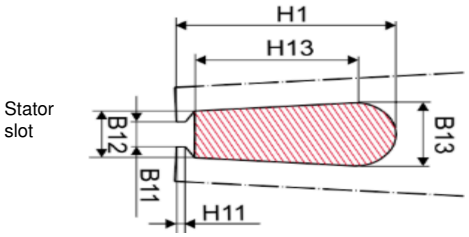

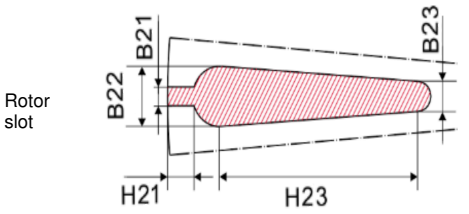

6 Simulation Results

For the online simulation, the pre-calculated inductances and resistances are used to calculate various performance parameters of the motor. The 2D matrices are called as a function of rotor position from 3D lookup tables using their index value.

The broken bars are simulated by adding a series resistance of 1 MΩ in-circuit editor of FEM in a commercial software called Infolytica with a considerable number of mesh elements with the inclusion of additional resistance and reactance to compensate the end windings. The same is done by increasing the resistance of the bar related entries (appendix I) in the resistance matrix of the proposed model, which is made using the equivalent rotor circuit model, as shown in Fig 6. Since the inductances do not depend upon the resistance of the rotor bar, they do not need to be calculated again. The only change in the respective elements of the resistance matrix can simulate the broken bar case, which reduces the simulation time. The rotor speed under healthy and broken rotor bar conditions is shown in Fig 7.

Both FEM and analytical simulations are performed at rated load conditions with motor specifications given in Table 3 and the results are shown in the steady-state regime.

Both speed and torque waveforms, calculated using FEM and proposed analytical model, are in good agreement with each other. The visible oscillations under healthy conditions are because of the winding and the rotor slot harmonics. Under the broken rotor bar cases, the increase in the amplitude of speed ripples with the increase in the number of broken rotor bars is evident in both cases. This oscillation is responsible for generating the right side harmonic (RSH) in the current spectrum. The 2D FEM model is solved for 2 s, equivalent to 100 periods, with a time-stepping of 0.033 ms, corresponding to a

Table 3 Motor specifications

Parameters	Symbol	Value
Rated speed	Nr	1400 rpm @ 50 Hz
Rated power	Pr	18 kW @ 50 Hz
Connection	—	Star (Y)
Power factor	cosϕ	0.860
Number of poles	p	4
Number of rotor bars	nb	40
Number of stator slots	Qs	48

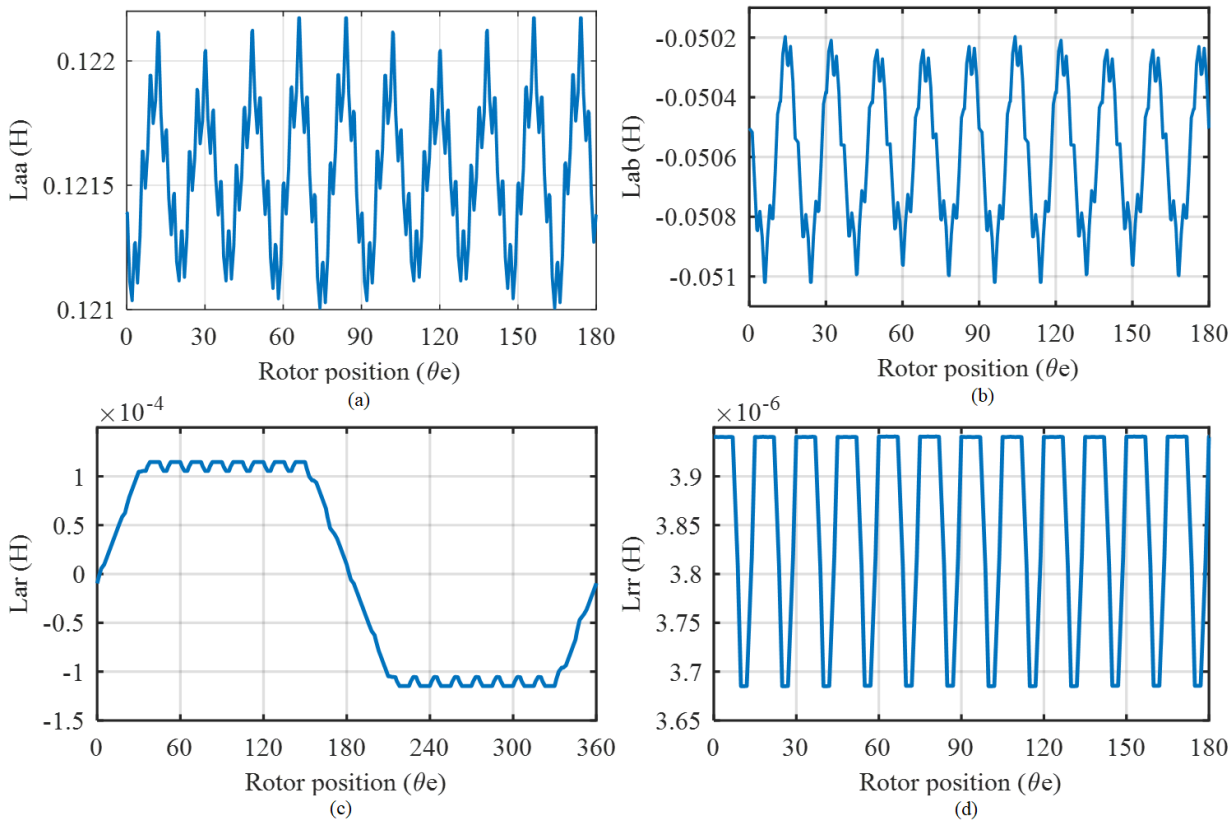

Fig. 4: The calculated inductances, (a) stator to stator self (L_{aa}), (b) stator to stator mutual (L_{ab}), (c) stator to rotor (L_{ar}), and (d) rotor to rotor (L_{rr}) with respect to the rotor position.

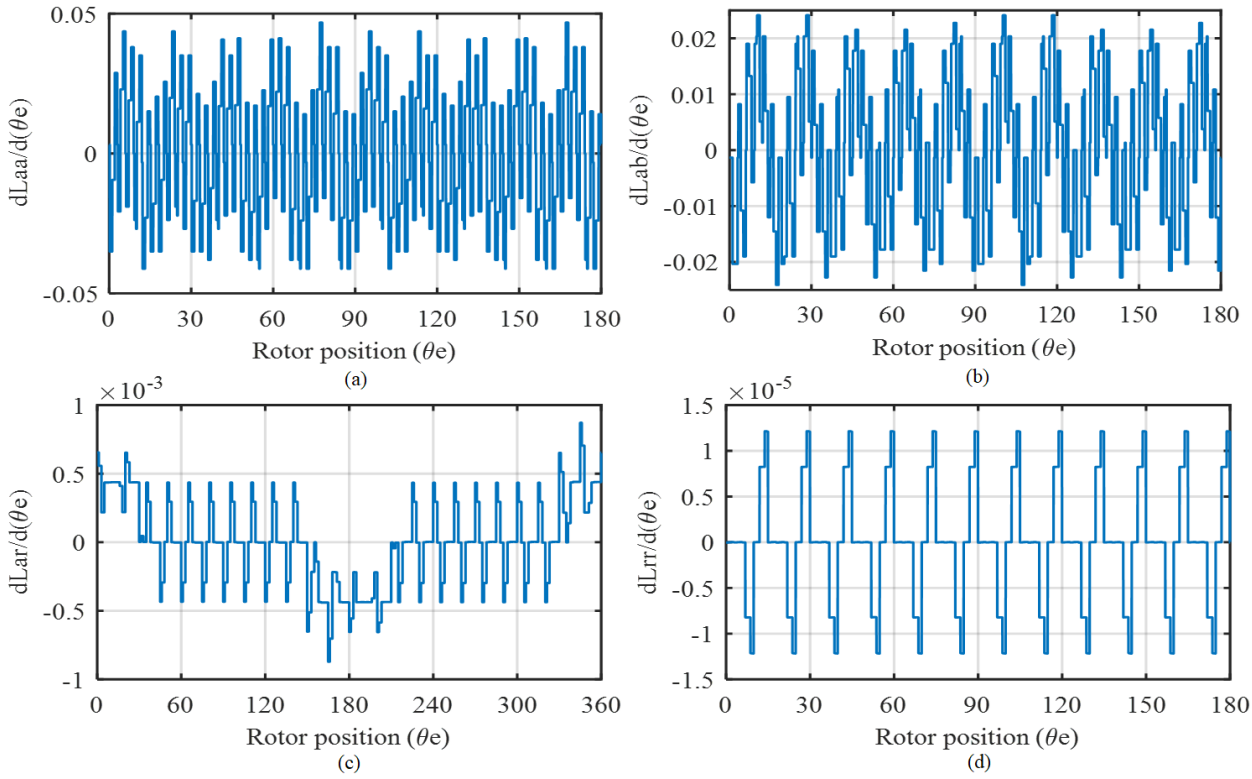

Fig. 5: The derivative of the, (a) stator to stator self (L_{aa}), (b) stator to stator mutual (L_{ab}), (c) stator to rotor (L_{ar}), and (d) rotor to rotor (L_{rr}) with respect to the rotor position.

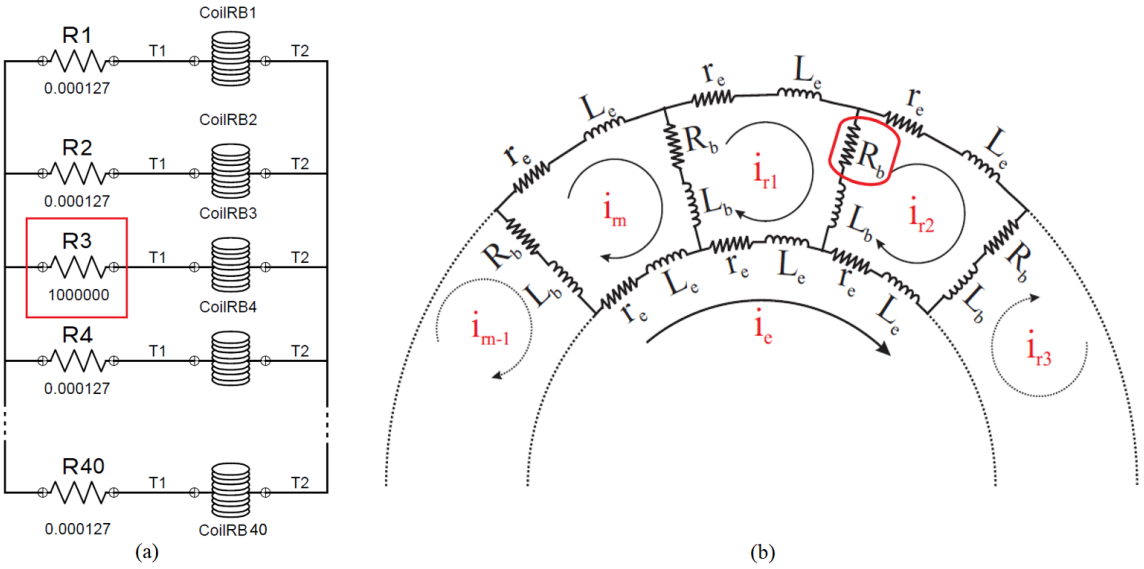

Fig. 6: The rotor schematic diagram with broken bar (a) in Infolytica circuit editor, and (b) in the proposed model.

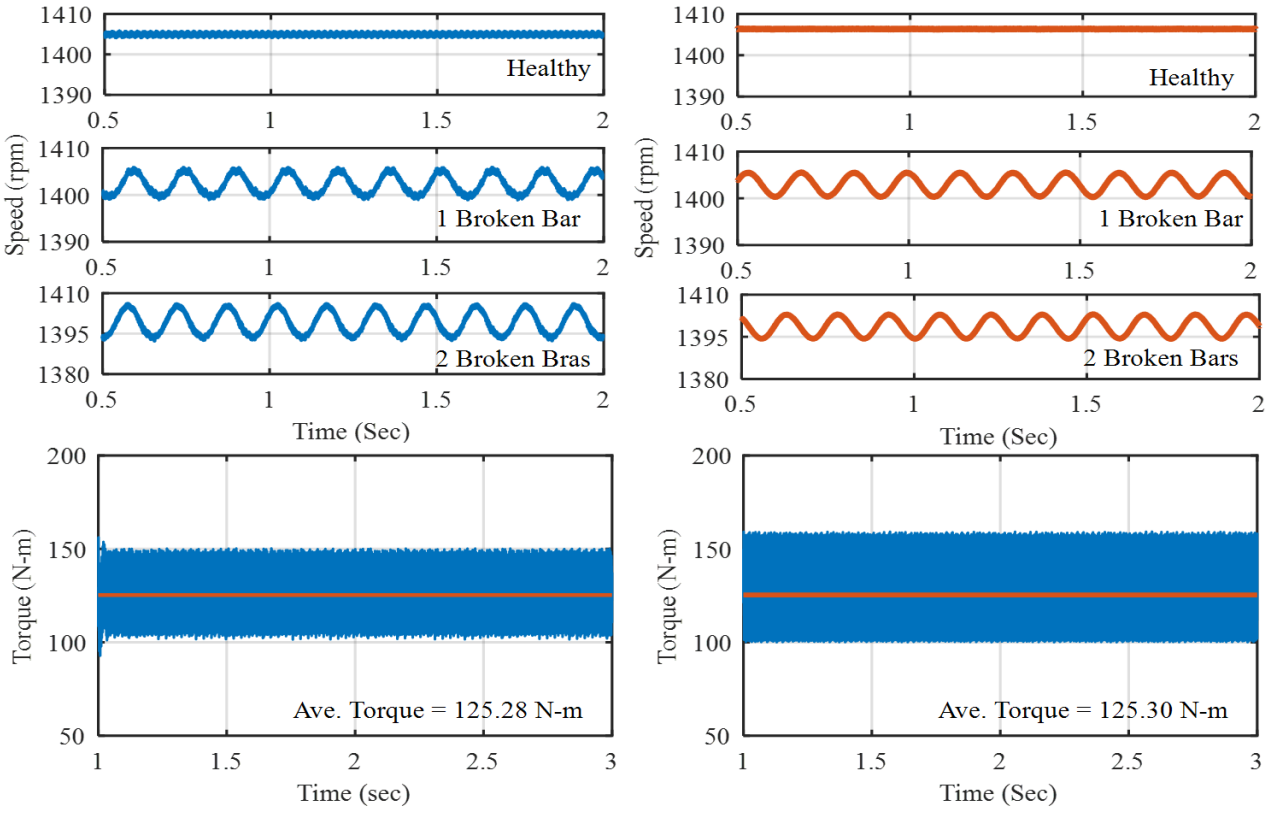

Fig. 7: The simulated speed and torque under healthy and broken rotor bar cases using FEM (left) and the proposed model (right).

sampling frequency of about 30 kHz. It takes about 0.7 s to calculate each step and about 12 h for a total of 60000 time steps with the computer specifications given in Table 4. The proposed analytical model calculates all parameters in just 3 minutes including both offline and online calculations with the same sampling frequency. The FEM model needs to be simulated again each time for each broken rotor bar case. But in the proposed model only the change in the resistance matrix is enough, which reduces the complexity considerably. Moreover, the most of the faults can be simulated in the online portion without going through the offline calculations again. By exploiting these facts, the model speed can be increased considerably which is very crucial for diagnostic algorithms.

7 Practical Measurement Setup

For practical measurements, two similar machines are connected back to back on a common mechanical foundation as shown in Fig.

Table 4 The comparison of the simulation time

Model	Computer specs	Simulation time
MWFA	Intel(R) Core(TM) i7-7500 CPU	3 minutes
FEM		12 hrs (1-time step / 0.72 Sec)

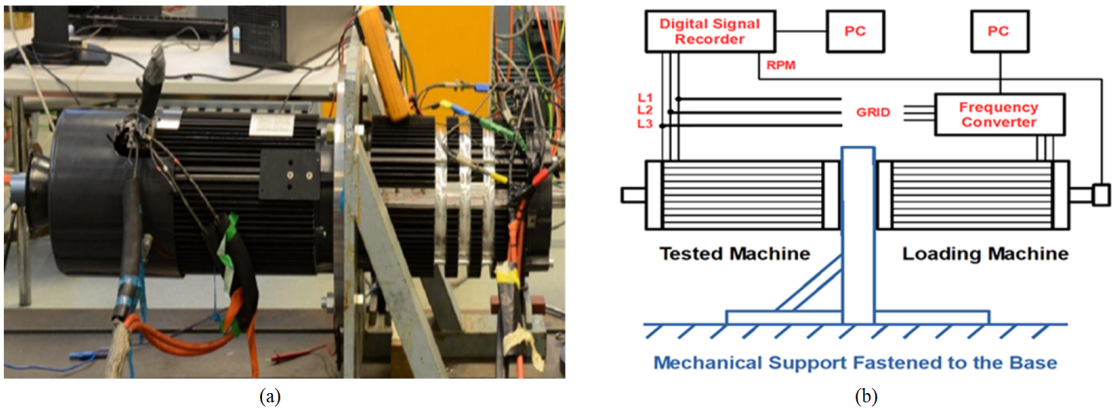

Fig. 8: (a) The laboratory setup for measurement, (b) the block diagram of the test rig.

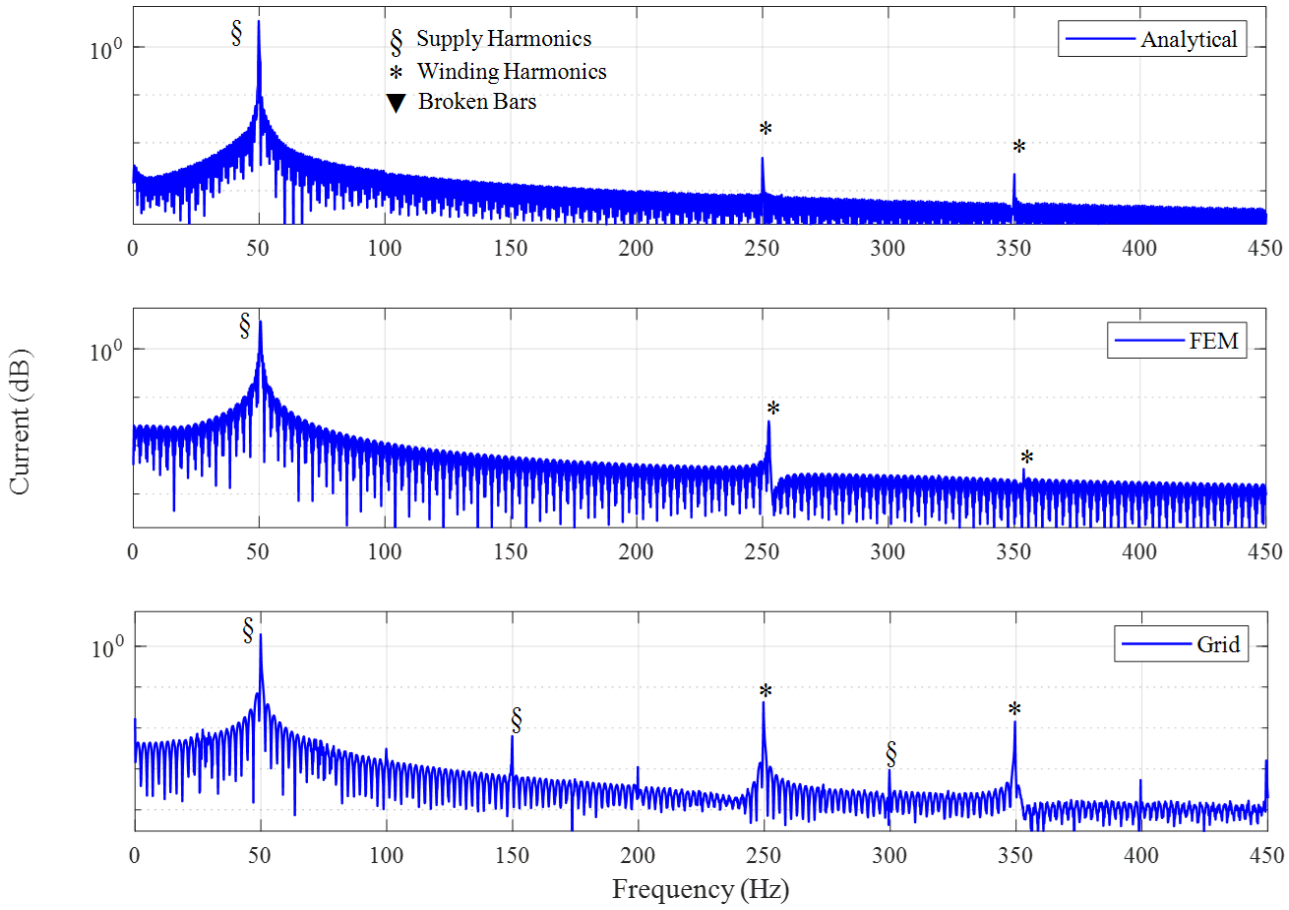

Fig. 9: The frequency spectrum (0-450 Hz) of the stator current using the proposed model, FEM and practical measurements from top to bottom in healthy and no-load cases.

8. One motor acts as a loading machine, which is being fed with an industrial inverter for better accuracy and slip controllability. The load side inverter is working under scalar mode to have less impact as in the case of direct torque control (DTC) mode. The motor under investigation is fed from the grid, while using the star connection scheme. The rotors with broken bars are prepared by drilling radial holes of equivalent length and width in them. The stator phase currents are measured with a sampling frequency of 10 kHz until 60 s for better frequency resolution. The measurements are taken under healthy, one, two, and three broken bar cases.

8 Validation of Results using The Frequency Spectrum

For validation, the frequency spectrum of the stator current simulated using the proposed model, FEM, and measured from test rig, is compared. The harmonics visible in the motor current spectrum are caused by various reasons but the most prominent causes are: the winding distribution, the stator, and rotor slot openings, asymmetry due to any fault, non-linear material characteristics and the supply. These harmonics give rise to the speed and torque ripples, increase eddy current and hysteresis losses and decrease efficiency. Since majority of the higher-order harmonics are slip dependent, they can be used constructively for sensor-less speed estimation at least under

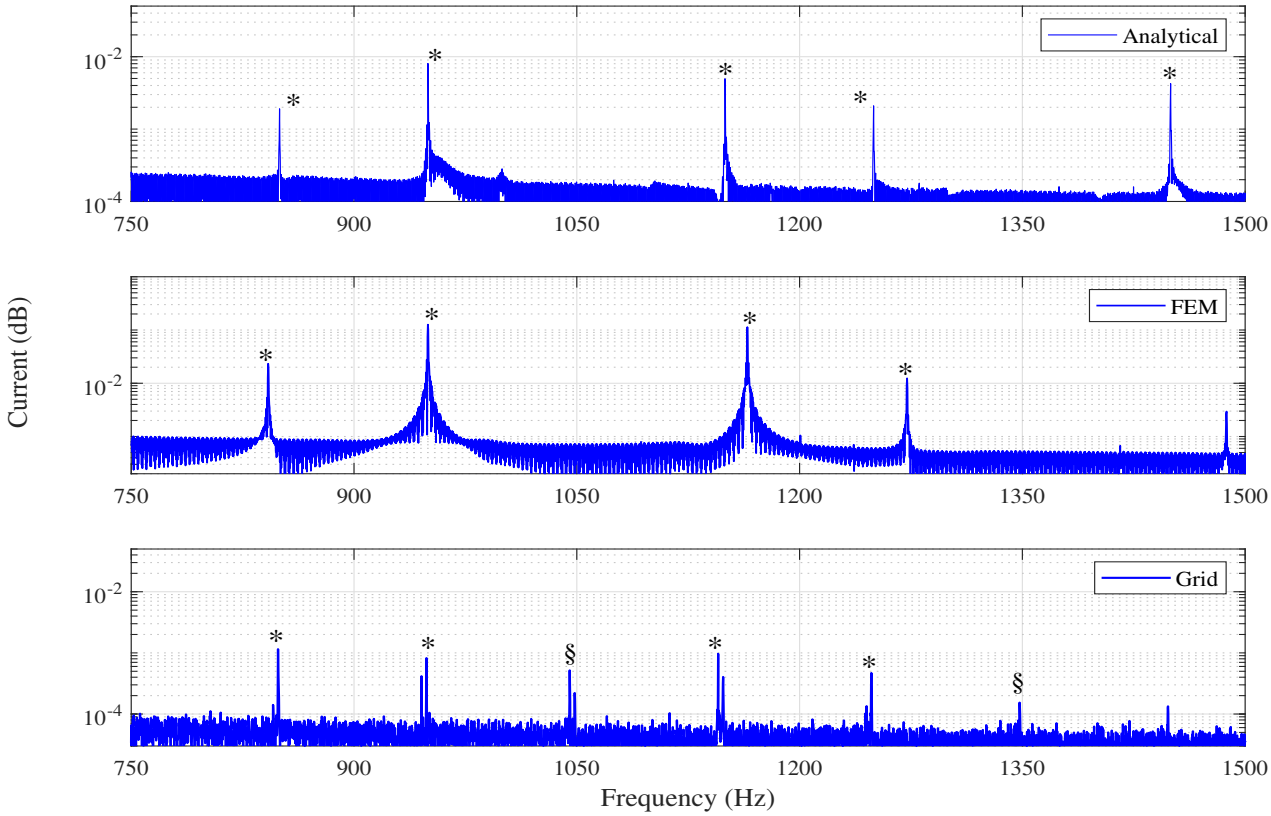

Fig. 10: The frequency spectrum (750-1500 Hz) of the stator current using the proposed model, FEM and practical measurements from top to bottom in healthy and no-load cases.

steady state regime. The harmonics until 450 Hz are presented in Fig. 9.

Since the winding configuration is stepped distributed, the odd multiples of fundamental components are clearly visible and are in good agreement with FEM and measurement-based results. In the case of experimental measurement based spectrum, some additional components are apparent because of the grid fed harmonics [3]. Similarly, the frequencies from 750 Hz to 1500 Hz are presented in Fig. 10, where the winding harmonics at 850 Hz, 950 Hz, 1150 Hz and 1250 Hz are evident in case of all analytical, FEM and practical measurements. These frequencies are present mainly because of the rotor slot harmonics, also called principal slot harmonics (PSH).

Since these results are at no load under healthy conditions, all components are at odd multiples of fundamental frequency and tend to move with the change in load. The development of the left side harmonic (LSH) at 43.4 Hz and the right side harmonic (RSH) at 53.5 Hz is due to broken rotor bars at rated load conditions, as presented in Fig. 11. The fault based frequency components can be defined using the equation VI in appendix.

In case of FEM, the RSH is absent since the measurements are based on a 2D model, where the effect of speed ripples is neglected. Similarly, the frequency spectrum related with principle slot harmonics at rated load and broken rotor bar conditions is shown in Figs. 12 and 13. The comparison of frequency spectra from the perspective of fault diagnostic reveals that the utilization of higher-order harmonics can be a better choice for the condition monitoring of the machine.

This is because of the fact that the fundamental component, being the strongest, has the largest spectral leakage as compared to the higher-order slotting harmonics. This means that under low-speed conditions the RSH and LSH are more likely to be buried under the fundamental component. This impact is small in case of PSH, which makes the model more suitable for fault diagnostic algorithms. The frequency spectra are studied using simple discrete time Fourier transform (DTFT) with a sampling frequency of 30 kHz. The

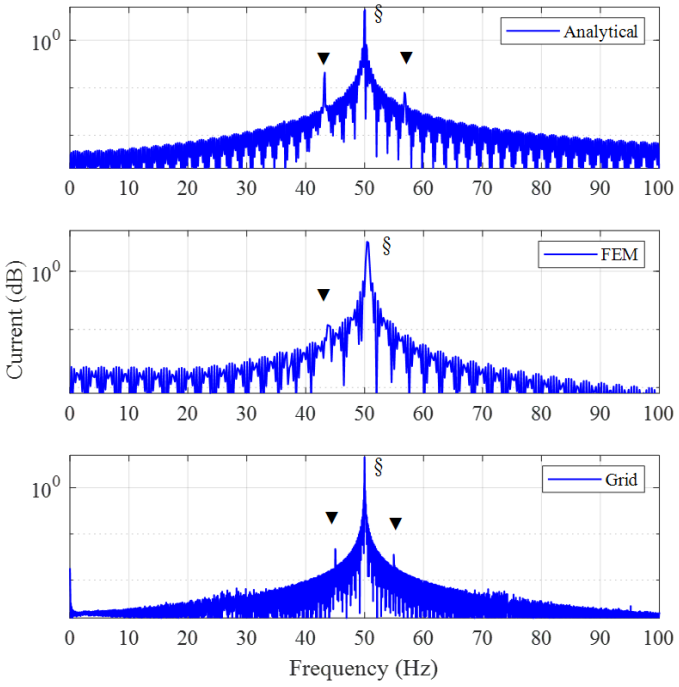

Fig. 11: The frequency spectrum (0-100 Hz) representing LSH and RSH under broken rotor bar at rated load condition.

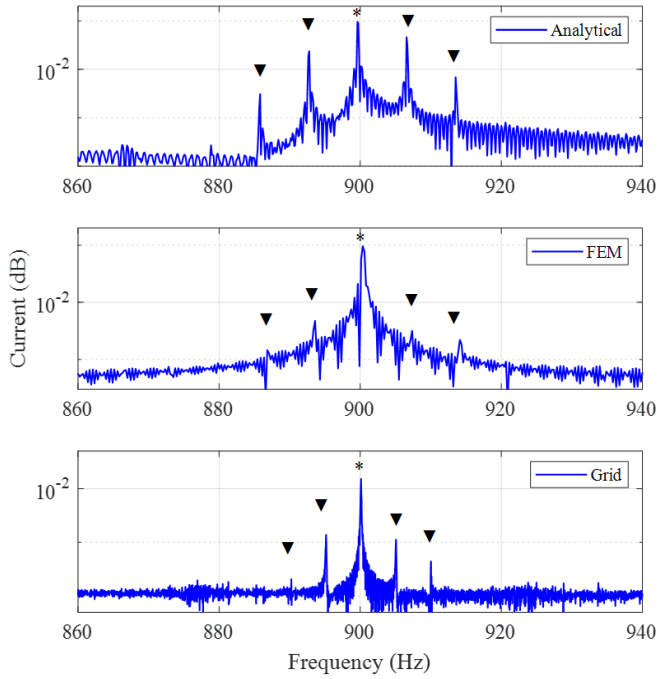

Fig. 12: The principal slot harmonic with subsequent broken bar frequencies showing less spectral leakage as compared to the fundamental component.

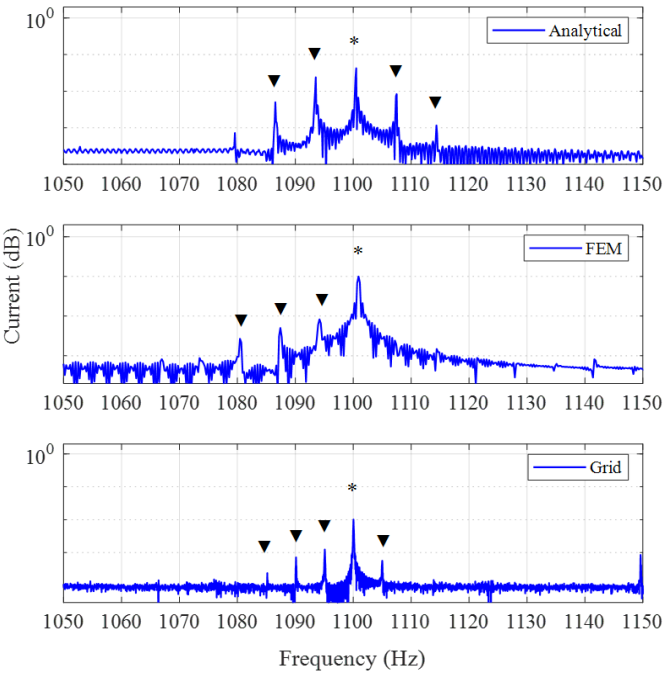

Fig. 13: The higher order spatial harmonics with broken rotor bar based frequencies.

spectral leakage is reduced by exploiting the benefits of Hamming window.

9 Conclusions

In this paper, a detailed time-stepping analytical model of a squirrel cage induction motor using MWFA is presented, with following attractive features:

Unlike most of the papers cited previously, where only low order harmonics are taken into account in the form of Fourier summation of certain sinusoids having specific frequency and amplitude. The actual stator and rotor winding functions are defined in the form of conditional analytical expressions.This approach makes the model independent of the selective number of frequency components and do not limit the spectrum bandwidth.

The air gap is made as a function of rotor and stator slot openings, which includes the spatial harmonics. Moreover, the inclusion of the air gap as a function of stator and rotor angles, makes the model suitable for the implementation of air gap related faults, such as eccentricity.

The inclusion of rotor slot harmonics makes the model suitable for sensor-less speed drive systems. The fact that these harmonics have less spectral leakage as compared to the fundamental component, makes them a potential candidate for fault detection, even under fewer load conditions.

The model is so generic that most of the fault types, such as broken rotor bars, static and dynamic eccentricity, and stator short circuits, can be simulated.

The very small simulation time, as compared to that used by FEM, makes the model suitable for advanced diagnostic algorithms, such as iterations based estimation of design parameters, hardware-in-the-loop, inverse problem theory, and other model-based diagnostic procedures.

The model is also suitable for the iterative optimization of various design parameters, such as winding functions, slot openings, and air gap, etc. The achieved results are in good agreement with the ones taken from the FEM model and laboratory measurements.

The separate modeling and simulation parts can further reduce the complexity and calculation time in the way that once the inductances are calculated, almost all kind of faults can be simulated by making corresponding changes in them .

10 References

[1] T. Wang, H. Liu, L. Zhao, J. Huang, and Z. Hou, 'Quantitative broken rotor bar fault detection for closed-loop controlled induction motors', IET Electr. Power Appl.,2016,10,(5), pp. 403–410.

[2] Z. Hou, J. Huang, H. Liu, M. Ye, Z. Liu, and J. Yang, 'Diagnosis of broken rotor bar fault in open- and closed-loop controlled wye-connected induction motors using zero-sequence voltage', IET Electr. Power Appl., 2017,11,(7), pp. 1214–1223.

[3] B. Asad, T. Vaimann, A. Belahcen, A. Kallaste, A. Rassõlkin, and M. N. Iqbal, 'Broken rotor bar fault detection of the grid and inverter-fed induction motor by effective attenuation of the fundamental component', IET Electr. Power Appl., Jul. 2019, pp. 1-10.

[4] Y. Park et al., 'Stray flux monitoring for reliable detection of rotor faults under the influence of rotor axial air ducts', IEEE Trans. Ind. Electron., vol. 66, no. 10, Oct. 2019 pp. 7561–7570.

[5] H. A. Toliyat, E. Levi, and M. Raina, 'A review of RFO induction motor parameter estimation techniques', IEEE Trans. Energy Convers., vol. 18, no. 2, Jun. 2003, pp. 271–283.

[6] P. C. Krause and C. H. Thomas, 'Simulation of Symmetrical Induction Machinery', IEEE Trans. Power Appar. Syst., vol. 84, no. 11, Nov. 1965, pp. 1038–1053.

[7] R. J. Lee, P. Pillay, and R. G. Harley, 'D-Q reference frames for the simulation of induction motors', Electr. Power Syst. Res., vol. 8, no. 1, Oct. 1984, pp. 15–26.

[8] A. R. Munoz and T. A. Lipo, 'Complex vector model of the squirrel-cage induction machine including instantaneous rotor bar currents', IEEE Trans. Ind. Appl., vol. 35, no. 6, 1999, pp. 1332–1340.

[9] C. C. M. Cunha, V. B. S. Varejao, and B. J. C. Filho, 'Simple model for squirrel cage induction machine with rotor asymmetries

and its validation through experimental tests on a special motor', in 2008 34th Annual Conference of IEEE Industrial Electronics, 2008, pp. 1385–1390.

[10] C. C. M. Cunha, R. O. C. Lyra, and B. Filho, 'Simulation and Analysis of Induction Machines With Rotor Asymmetries', IEEE Trans. Ind. Appl., vol. 41, no. 1, Jan. 2005, pp. 18–24.

[11] M. Jannati, N. R. N. Idris, and Z. Salam, 'A new method for modeling and vector control of unbalanced induction motors', in 2012 IEEE Energy Conversion Congress and Exposition (ECCE), 2012, pp. 3625–3632.

[12] D. C. Patel and M. C. Chandorkar,'Transient modeling and analysis of induction motors with position effects in stator turn faults', in 2010 IEEE International Conference on Industrial Technology, 2010, pp. 1251–1256.

[13] J. Milimonfared, H. M. Kelk, S. Nandi, A. D. Minassians, and H. A. Toliyat, 'A novel approach for broken-rotor-bar detection in cage induction motors', IEEE Trans. Ind. Appl., vol. 35, no. 5, 1999, pp. 1000–1006.

[14] H. A. Toliyat and T. A. Lipo, 'Transient analysis of cage induction machines under stator, rotor bar and end ring faults', IEEE Trans. Energy Convers., vol. 10, no. 27, Jun. 1995, pp. 241–24.

[15] G. M. Joksimovic and J. Penman, 'The detection of inter-turn short circuits in the stator windings of operating motors', IEEE Trans. Ind. Electron., vol. 47, no. 5, 2000, pp. 1078–1084.

[16] J. Faiz and M. Ojaghi, 'Unified winding function approach for dynamic simulation of different kinds of eccentricity faults in cage induction machines', IET Electr. Power Appl., vol. 3, no. 5, 2009, p. 461-470.

[17] H. A. Toliyat, M. S. Arefeen, and A. G. Parlos, 'A method for dynamic simulation of air-gap eccentricity in induction machines', IEEE Trans. Ind. Appl., vol. 32, no. 4, 1996, pp. 910–918.

[18] G. Y. Sizov, Chia-Chou Yeh, and N. A. O. Demerdash, 'Magnetic equivalent circuit modeling of induction machines under stator and rotor fault conditions', in 2009 IEEE International Electric Machines and Drives Conference, 2009, pp. 119–124.

[19] S. D. Sudhoff, B. T. Kuhn, K. A. Corzine, and B. T. Branecky, 'Magnetic Equivalent Circuit Modeling of Induction Motors', IEEE Trans. Energy Convers., vol. 22, no. 2, Jun. 2007, pp. 259–270.

[20] A. Mahyob, M. Y. O. Elmoctar, P. Reghem, and G. Barakat, 'Induction machine modeling using Permeance Network Method for dynamic simulation of air-gap eccentricity', in 2007 European Conference on Power Electronics and Applications, 2007, pp. 1–9.

[21] J. Apsley and S. Williamson, 'Analysis of multiphase induction machines with winding faults', IEEE Trans. Ind. Appl., vol. 42, no. 2, Mar. 2006, pp. 465–472.

[22] S. Williamson and E. R. Laithwaite, 'Generalised harmonic analysis for the steady-state performance of sinusoidally-excited cage induction motors', IEE Proc. B Electr. Power Appl., vol. 132, no. 3, 1985, pp. 157-163.

[23] S. Williamson and S. Smith, 'Pulsating torque and losses in multiphase induction machines', IEEE Industry Applications Conference. 36th IAS Annual Meeting (Cat. No.01CH37248), vol. 2, 2001, pp. 1155–1162.

[24] S. Bachir, S. Tnani, J.-C. Trigeassou, and G. Champenois, 'Diagnosis by parameter estimation of stator and rotor faults occurring in induction machines', IEEE Trans. Ind. Electron., vol. 53, no. 3, Jun. 2006, pp. 963–973.

[25] L. Wang, J. Jatskevich, and S. D. Pekarek, 'Modeling of Induction Machines Using a Voltage-Behind-Reactance Formulation', IEEE Trans. Energy Convers., vol. 23, no. 2, Jun. 2008, pp. 382–392.

[26] A. Sapena-Bano, J. Martinez-Roman, R. Puche-Panadero, M. Pineda-Sanchez, J. Perez-Cruz, and M. Riera-Guasp, 'Induction machine model with space harmonics for fault diagnosis based on the convolution theorem', Int. J. Electr. Power Energy Syst., vol. 100, Sep. 2018, pp. 463–481.

[27] A. Belahcen, A. Arkkio, and J. Martinez, 'Broken bar indicators for cage induction motors and their relationship with the number of consecutive broken bars',IET Electr. Power Appl., vol. 7, no. 8, Sep. 2013, pp. 633–642.

[28] J. Faiz, B. M. Ebrahimi, H. A. Toliyat, and W. S. Abu-Elhaija, 'Mixed-fault diagnosis in induction motors considering varying load and broken bars location', Energy Convers. Manag., vol. 51, no. 7, Jul. 2010, pp. 1432–1441.

[29] Z. Song, Y. Yu, F. Chai, and Y. Tang, 'Radial Force and Vibration Calculation for Modular Permanent Magnet Synchronous Machine With Symmetrical and Asymmetrical Open-Circuit Faults', IEEE Trans. Magn., vol. 54, no. 11, Nov. 2018, pp. 1–5.

[30] V. Fireteanu, 'Detection of the Short-Circuit Faults in the Stator Winding of Induction Motors Based on Harmonics of the Neighboring Magnetic Field', J. Phys. Conf. Ser., vol. 450, Jun. 2013, pp. 1-7.

[31] J. Martinez, A. Belahcen, J. Detoni, and A. Arkkio, 'A 2D FEM analysis of electromechanical signatures in induction motors under dynamic eccentricity', Int. J. Numer. Model. Electron. Networks, Devices Fields, vol. 27, no. 3, May 2014, pp. 555–571.

[32] B. M. Ebrahimi, J. Faiz, and M. J. Roshtkhari, 'Static-, Dynamic-, and Mixed-Eccentricity Fault Diagnoses in Permanent-Magnet Synchronous Motors', IEEE Trans. Ind. Electron., vol. 56, no. 11, Nov. 2009, pp. 4727–4739.

[33] H. A. Toliyat, T. A. Lipo, and J. C. White, 'Analysis of a concentrated winding induction machine for adjustable speed drive applications. I. Motor analysis', IEEE Trans. Energy Convers., vol. 6, no. 4, 1991, pp. 679–683.

[34] H. A. Toliyat, T. A. Lipo, and J. C. White, 'Analysis of a concentrated winding induction machine for adjustable speed drive applications. II. Motor design and performance', IEEE Trans. Energy Convers., vol. 6, no. 4, 1991, pp. 684–692.

[35] A. M. El-Refaie, T. M. Jahns, and D. W. Novotny, 'Analysis of Surface Permanent Magnet Machines With Fractional-Slot Concentrated Windings', IEEE Trans. Energy Convers., vol. 21, no. 1, Mar. 2006, pp. 34–43.

[36] J. Faiz and I. Tabatabaei, 'Extension of winding function theory for nonuniform air gap in electric machinery', IEEE Trans. Magn., vol. 38, no. 6, 2002, pp. 3654–3657.

[37] S. Nandi, 'Modeling of Induction Machines Including Stator and Rotor Slot Effects', IEEE Trans. Ind. Appl., vol. 40, no. 4, Jul. 2004, pp. 1058–1065.

[38] A. Marfoli, P. Bolognesi, L. Papini, and C. Gerada, 'Mid-Complexity Circuital Model of Induction Motor with Rotor Cage: A Numerical Resolution', in 2018 XIII International Conference on Electrical Machines (ICEM), 2018, pp. 277–283.

[39] J. Pippuri and A. Arkkio, 'Time-Harmonic Induction-Machine Model Including Hysteresis and Eddy Currents in Steel Laminations', IEEE Trans. Magn., vol. 45, no. 7, Jul. 2009, pp. 2981–2989.

[40] A. Kumar, S. Marwaha, A. Marwaha, and N. S. Kalsi, 'Magnetic field analysis of induction motor for optimal cooling duct design', Simul. Model. Pract. Theory, vol. 18, no. 2, Feb. 2010, pp. 157–164.

[41] J. Martinez, A. Belahcen, and J. G. Detoni, 'A 2D magnetic and 3D mechanical coupled finite element model for the study of the dynamic vibrations in the stator of induction motors', Mech. Syst. Signal Process., vol. 66–67, Jan. 2016, pp. 640–656.

[42] Ranran Lin and A. Arkkio, '3-D Finite Element Analysis of Magnetic Forces on Stator End-Windings of an Induction Machine', IEEE Trans. Magn., vol. 44, no. 11, Nov. 2008, pp. 4045–4048.

[43] J. Pyrhonen, T. Jokinen, and V. Hrabovcova, Design of rotating electrical machines. Wiley, 2008.

11 Appendices

The broken rotor bars can be simulated by changing the resistance values of the related entries in the resistance matrix. The red elements in the equation shown below represent the values need to be changed to simulate second rotor bar. The conversion of integral based equations into mean functions as in (II)-(V), makes their implementation easier.

$$R_{rr} = \begin{bmatrix} 2(R_b+r_e) & -R_b & 0 & 0 & \cdots & 0 & \cdots & 0 & -R_b & -r_e \\ -R_b & 2(R_b+r_e) & -R_b & 0 & \cdots & 0 & \cdots & 0 & 0 & -r_e \\ 0 & -R_b & 2(R_b+r_e) & -R_b & \cdots & 0 & \cdots & 0 & 0 & -r_e \\ \vdots & \vdots & \vdots & \vdots & \vdots & \vdots & \vdots & \vdots & \vdots & \vdots \\ 0 & 0 & 0 & 0 & \cdots & 0 & \cdots & 2(R_b+r_e) & -R_b & -r_e \\ -R_b & 0 & 0 & 0 & \cdots & 0 & \cdots & -R_b & 2(R_b+r_e) & -r_e \\ -r_e & -r_e & -r_e & -r_e & \cdots & -r_e & \cdots & -r_e & -r_e & n_b r_e \end{bmatrix} \quad \text{(I)}$$

$$L_{ij}(\theta) = \mu_o r l \int_0^{2\pi} P(\phi,\theta) N_i(\phi,\theta) n_j(\phi,\theta) d\theta \quad \text{(II)}$$

$$L_{ij}(\theta) = 2\pi\mu_o r l \frac{1}{2\pi} \int_0^{2\pi} P(\phi,\theta) N_i(\phi,\theta) n_j(\phi,\theta) d\theta \quad \text{(III)}$$

Since the definition of mean function is:

$$< f >= \frac{1}{2\pi} \int_0^{2\pi} f(\theta).d\theta \quad \text{(IV)}$$

Therefore;

$$L_{ij}(\theta) = 2\pi\mu_o r l < P(\phi,\theta) N_i(\phi,\theta) n_j(\phi,\theta) > \quad \text{(V)}$$

$$f_{BR} = f_s \pm 2ksf_s, \quad k = 1, 2, 3, ... \quad \text{(VI)}$$

Where f_{BR}, f_s and s are the broken rotor bars based frequencies, supply fundamental frequency and the slip respectively.
The leakage inductance of end winding can be calculated as [43]:

$$L_{ew} = \frac{Q_s}{m} q \left(\frac{Z_q}{a}\right)^2 \mu_o l_w \lambda_w \quad \text{(VII)}$$

Where Q_s is the number of slots, Z_q is the number of conductors per slot, m is the number of stator phases, a are the number of parallel paths per phase, q is number of slots per pole and phase, μ_o is the permeability of free space, l_w is the average length of winding outside of the stator and λ_w is the permeance factor which is 0.20 for motor under investigation.
The stator and the rotor turn functions can be defined as:

$$n_{as}(\theta) = \begin{cases} Z_q * i, & i = 1:1:Q_{pp} \\ Z_q * Q_{pp}, & i = (Q_{pp}+1):1:3*Q_{pp} \\ Z_q(Q_{pp}-1), & i = (3*Q_{pp}+1):1:4*Q_{pp} \\ 0, & i = (4*Q_{pp}+1):1:2*Q_s/p \end{cases} \quad \text{(VIII)}$$

$$n_r(\alpha) = \begin{cases} 1, & \theta_i \leqslant \alpha_e \leqslant \theta_i + \alpha_r \\ 0, & \theta_i > \alpha_e > \theta_i + \alpha_r \end{cases} \quad \text{(IX)}$$

Where Z_q is the number of conductors per stator slot, Q_{pp} is the number of slots per pole and phase, Q_s is the total number of stator slots and i is the integer. This conditional analytical function can be used to generate the turn function of stator phase winding. The remaining two turn functions can be produced by shifting it to $(2\pi/3)$ and $(4\pi/3)$ respectively. While, the rotor turn function can be represented as in (IX), where θ_i is the starting angle of rotor bar from a reference point and α_r is the angular displacement between two consecutive bars.